A false alarm reduction method for GPR sensor moving at varying heights

Sezgin, M., Nazlı, H., Özkan, E., Çelik, Esra

M. Sezgin, H. Nazlı, E. Özkan, Esra Çelik, "A false alarm reduction method for GPR sensor moving at varying heights," Proc. SPIE 11418, Detection and Sensing of Mines, Explosive Objects, and Obscured Targets XXV, 1141807 (29 April 2020); doi: 10.1117/12.2565907

SPIE.

Event: SPIE Defense + Commercial Sensing, 2020, Online Only

A FALSE ALARM REDUCTION METHOD FOR GPR SENSOR MOVING AT VARYING HEIGHTS

M. Sezgin*[a], H. Nazlı[a], E. Özkan[a], Esra Çelik[a]
[a] TÜBİTAK BİLGEM, Gebze KOCAELİ TURKEY

ABSTRACT

In this study, we present a brief information about GPR data processing and then processing methods are proposed dedicated to false alarm reduction with varying antenna height. We used horizontal filtering in cross-track and continuous wavelet transformation for A-scan signals. Additionally, 2D Wavelets and Gabor filters are applied to the data. Comparative results are presented over real data set obtained from various buried objects. It is observed that the horizontal filtering gives satisfactory results especially in cases where there is variability in antenna height.

Keywords: GPR, clutter reduction, false alarm reduction, preprocessing

1. INTRODUCTION

Ground Penetrating Radar (GPR) applications take place in civilian and military areas. There are many factors that affect GPR system performance [1], radiated power, transmitted signal modulation type, signal bandwidth, electromagnetic properties of the buried object (dielectric coefficient, loss, conductivity, etc.), properties of the medium to be inspected (dielectric coefficient, loss, conductivity, etc.), antenna gain and pattern, spatial data collection method, change of distance between antenna and soil surface and signal processing methods directly affects the performance of GPR.

GPR systems can be realized in frequency domain or time domain [1]. In each category there are different difficulties. In time domain systems, alignment of sequential A-scan signals is one of the important problems in data collection stage, it may increase false alarm rate in rough surfaces if it is not properly tuned. At the same time, rough surfaces or change in the height of the antenna to the ground may cause false alarms in GPR detection test statistic function (DTS) [2].

The antenna should be moved as close as possible to the ground surface to ensure efficient transmission from antenna to theground. However, when antenna-near field covers a part of the soil, the antenna characteristics change and low frequency components appear, which creates floating horizontal lines in B scan data corresponding to false alarms in DTS. There are studies in the literature that take into account the proximity of the antenna to the surface [3].

GPR Data processing can be categorized as anomaly detection and identification. Anomaly detection contains preprocessing, background removal/clutter reduction and detection test statistics calculation. Identification contains, visual interpretation of the data, feature extraction and classification.

In general, GPR data collection procedures can be categorized as controlled and uncontrolled. In controlled one, GPR A scan data is obtained sequentially according to a positioning sensor, such as wheel encoder or MEMS based positioning sensor. Most of the Geophysical GPR applications [4], railway base inspection [5], vehicle/robot-based applications [6] and some handheld mine detectors [7] can be considered in this category. On the other hand, the second group mainly consists of ordinary dual sensor mine detectors such as [8], [9].

For mine detection case GPR is one of the main sensors used in the detection and identification of metallic and non-metallic objects buried under the ground [10,11,12]. The detection and identification of the buried target depends on many natural parameters, such as soil dielectric properties, soil inhomogeneity, buried rocks, roots, and operating method of device [1]. Additionally, difficulties arise in systems that move very close to the ground and clutters caused by roughness of the soil surface and the user's inability to move the antenna always parallel to the surface cause false alarms in detection. In order to avoid these undesired effects and to reduce clutter, various pre-processing methods needs to be applied to the GPR data. In a GPR system developed for mine detection, it is particularly important to reduce the false alarm rate in detection. Elimination of the signal coming from the ground surface and prevention of false alarms caused by the change in antenna height also arises as a desired feature.

* mehmet.sezgin@tubitak.gov.tr; phone +90 262 675 3041; fax +90 262 646 3187.

Detection and Sensing of Mines, Explosive Objects, and Obscured Targets XXV, edited by Steven S. Bishop, Jason C. Isaacs, Proc. of SPIE Vol. 11418, 1141807 · © 2020 SPIE
CCC code: 0277-786X/20/$21 · doi: 10.1117/12.2565907

In order to solve this problem, a preprocessing method based on filtering at depth lines of GPR B-scan data and use of continuous wavelet transform over A-scan signals is presented. Additionally, use of 2-D wavelets and Gabor filter is applied to GPR data. Comparative results are also given over the actual data set obtained from various scenarios. We'll start with a brief introduction on GPR data processing and then the methods will be studied, at the end results of the methods will be given.

2. METHODOLOGY

In most applications, first step of buried object detection is pre-preprocessing [1]. Preprocessing stage may contain, filtering, alignment and averaging of A-scans to reduce undesired signals. After this step, background removal/ clutter reduction, then anomaly detection methods are applied. Anomaly detection methods can be realized based on prediction of the next A-scan signals from previous ones, calculation of the target energy by correlating the background removed A-scan signals in a window, etc. If the second method is used, we have constant or moving background signal calculation options [2]. If we calculate background signal estimation at the beginning near to the starting location this is named as constant background calculation, if we update this background as antenna moves along with cross-track this is named as moving background calculation. When we subtract this background estimation of A-scan signal from incoming A-scan signals, we obtain estimation of background removed B-scan data.

In this study our aim is to reduce false alarm rate and to obtain interpretable B-scan data simultaneously, even the antenna has varying heights. In varying antenna height situation, antenna near-field characteristics changes, which affects system performance, then low frequency components appear in GPR data which causes horizontally sliding lines (generates false alarms in DTS. We need to eliminate the clutter that occur in case of a change in antenna height. In this scope, we apply different background removal/clutter reduction methods, filtering on each horizontal line of B-scan data, wavelet filtering for A-scan signals, 2-D wavelets and Gabor filtering for 2-D data. We perform a comparison for the considered methods.

2.1 GPR target detection

A typical GPR data and DTS function are given in Figure-1. The coordinate system and a sample B-scan image is given in Figure-1(a) which is reconstructed by horizontal concatenation of A-scan signals given in Figure 1(d). Detection test statistic is plotted in Figure-1(c). Grid structure of B-scan data, background removal windows and correlation window is presented in Figure-1(b). In Figure-1(d), $a_x(z)$ represents the A-scan data acquired at position x, where z is the depth index. Background removed A-scan signal - $s_x(z)$ is obtained by (1), estimation of B-scan Data is calculated by (2), equation (3) express calculation of detection test statistics (DTS) [2], $b(z)$ represents background signal estimate. List of the studied methods are given in Table-1

$a_x(z)$: Raw A-scan signal (column vector) acquired at position x

$b(z)$: A-scan background signal estimate

$s_x(z)$: Raw A-scan target signal estimate at position x

N : Length of A-scan signal

M : Number of A-scan signal in B-Scan data

P : Background calculation window length

K : Number of A-scan signals to be correlated

$B(x,z)$: Raw 2-D GPR B-scan data

$\beta_z(x)$: z^{th} row of B scan data

$B_T(x,z)$: B-scan 2-D target data estimate

$DTS(x)$: Detection test statistics function

$$s_x(z) = a_x(z) - b(z) \quad (1)$$

$$B_T(x,z) = \{s_x(z)\},\ x = 1, \dots, M-1,\ z = 1, \dots, N-1 \quad (2)$$

$$DTS(x) = \sum_{k=1}^{K} max\{s_{x-k}(z) * s_x(z)\}\text{, where * represents convolution operator} \quad (3)$$

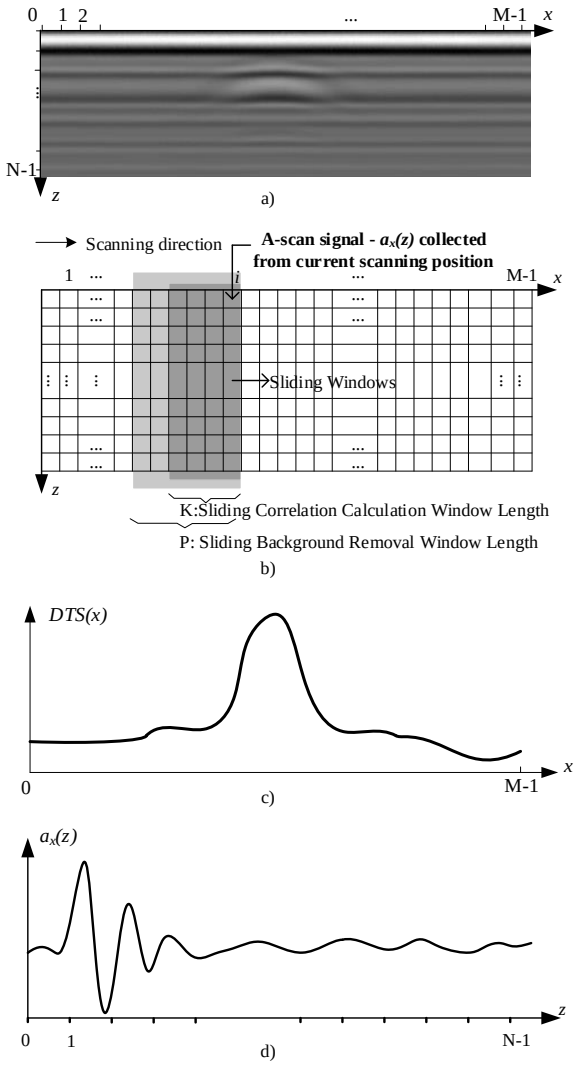

Figure-1. GPR data processing scenario, a) GPR B-scan data (reconstructed by horizontal concatenation of A-scan signals), b) data grid of GPR image c) detection test statistics - DTS, d) an example A-scan signal.

Table-1. The list of studied methods.

	Background removal	**Horizontal Filtering**	**Wavelet Filtering**	**Gabor filter**	**2-D Wavelet Transform**
Method-1	Constant	-	-	-	-
Method-2	Constant	Yes	-	-	-
Method-3	Moving	-	-	-	-
Method-4	Moving	Yes	-	-	-
Method-5	Constant	Yes	Meyer	-	-
Method-6	Moving	Yes	Meyer	-	-
Method-7	Constant	Yes	Haar	-	-
Method-8	Moving	Yes	Haar	-	-
Method-9	Constant	-	-	-	Yes
Method-10	Constant	Yes	-	-	Yes
Method-11	Constant	Yes	-	Yes	-
Method-12	Moving	Yes	-	Yes	-
Method-13	Constant	-	-	Yes	-

2.2 Pre-processing

Most of the time, digital filtering is applied to A-scan signals to remove undesired signal components at the beginning. In this study, we applied Butterworth band-pass filter to each A-scan signal as pre-processing with the parameters given in Table-2.

Table-2. Band-pass filter parameters of pre-processing.

First Stopband Frequency (normalized)	0.0040
First Passband Frequency (normalized)	0.0100
Second Passband Frequency (normalized)	0,0579
Second Stopband Frequency (normalized)	0.0921
First Stopband Attenuation	10 [dB]
Pass-band Ripple	1 [dB]
Second Stopband Attenuation	10 [dB]

2.3 Background removal

In constant background removal, an average A-scan is calculated from P A-scan signals at the beginning by taking average at each depth and this signal is subtracted from each A scan signal [2]. In moving average case, background signal estimate is updated dynamically as the position changes, this updated background signal is subtracted from each A scan signal, at the end background removed signal $B_T(x,z)$ is obtained. In our study constant or moving background removal is used according to Table-1, for each specified method.

2.4 Horizontal filtering

In order to remove varying height effect of antenna as much as possible, we applied a Butterworth high pass filter to each row of B-scan data. Filter parameters are given in Table-3 for a specific scanning speed. A sample is given in Figure-2, black line corresponds to a horizontal profile of B-Scan data $\beta_z(x)$, red line corresponds to high pass filtered horizontal profile of B-Scan data - $\beta'_z(x)$. As it is shown in Figure-2(c), horizontal sliding lines have been removed from B-scan data by using horizontal filtering.

Table-3. High-pass filter parameters of horizontal filtering.

Stopband Frequency (normalized)	0.0051
Passband Frequency (normalized)	0.0150
Stopband Attenuation	30 [dB]
Pass-band Ripple	1[dB]

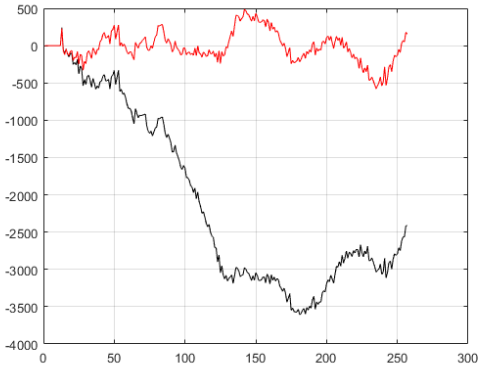

a) Black line: original signal ($\beta_z(x)$), red line: high pass filtered signal ($\beta'_z(x)$).

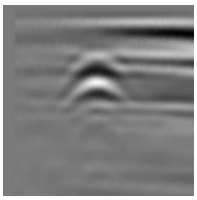

b) Processed B-scan data without horizontal filtering.

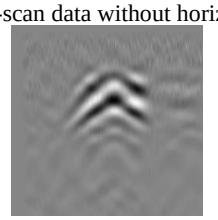

c) Processed B-scan data with horizontal filtering.

Figure-2 Effects of horizontal filtering.

2.5 Wavelet filtering

Continuous wavelets can be used to extract information from the data [13]. Unlike conventional Fourier analysis, it is possible to search for signals in a certain form with wavelet filtering. In this context, we used Meyer [14] wavelet to search the desired signal over A-scan signals. General expression of 1-D wavelet are given by (4). We used Meyer wavelet given in Figure-3

$$W(a,b) = \frac{1}{\sqrt{a}} \int_{-\infty}^{+\infty} x(t).\psi\left(\frac{t-b}{a}\right) dt \tag{4}$$

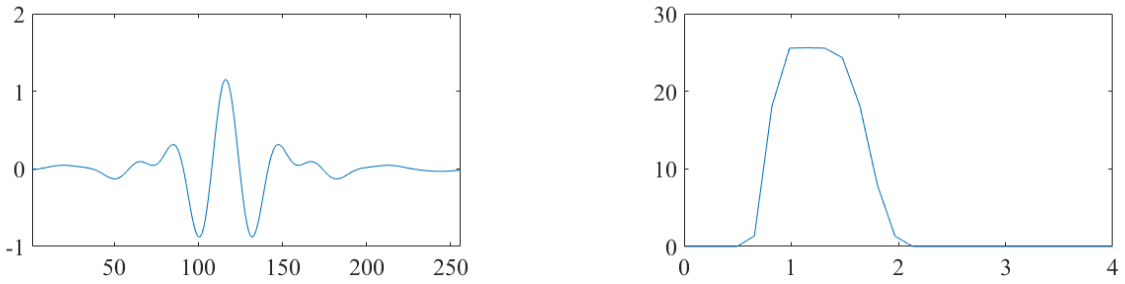

a) Meyer wavelet. b) Frequency spectrum of Meyer Wavelet.

Figure-3 1-D Continuous wavelet and frequency spectrum

2.6 Wavelet Denoising

Since wavelets localize features in different scales, undesired part of the signal can be removed by keeping important signal features. The basic idea behind wavelet denoising, or wavelet thresholding, is that the wavelet transform leads to a sparse representation for many real-world signals [13]. Wavelet coefficients which are small in value are typically noise and we can "shrink" those coefficients without degradation in signal. After we threshold the coefficients, we reconstruct the data using the inverse wavelet transform. In this processing method, we applied the wavelet denoising to GPR A-Scan signals by using Haar wavelet by selecting decomposition level-3 with universal soft thresholding and rescaling using level-dependent estimation of level noise. A typical Haar wavelet is given in the following figure for a specific level.

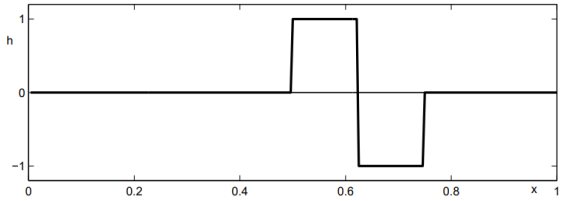

Figure-4 A typical 1-D Haar wavelet representation.

2.7 2-D wavelet

The 2-D continuous wavelet transform [14], [15] is a representation of 2-D data in variables: dilation, rotation, and position. Dilation and rotation are real-valued scalars and position is a 2-D vector with real-valued elements. In proper conditions, the 2-D CWT is defined by (5). We applied 2-D wavelet transform to GPR B-scan data by using gauss wavelet. Scale parameter 4 is used. A sample result of 2-D Continuous wavelet is given Figure-5.

a) Original GPR B-scan data. b) 2-D wavelet representation.

Figure-5 2-D Continuous wavelet representation of GPR data.

$$WT_f(a,b,\theta) = \int_{\mathbb{R}^2} f(x)\frac{1}{a}\bar{\psi}(r_{-\theta}\left(\frac{x-b}{a}\right)dx\ ,\ a \in \mathbb{R}^+, x, b \in \mathbb{R}^2\ , r_\theta = \begin{pmatrix}\cos(\theta) & -\sin(\theta)\\ \sin(\theta) & \cos(\theta)\end{pmatrix}\ \theta \in [0,2\pi) \quad (5)$$

2.8 Gabor filtering

Gabor filter [16] is a linear filter used for texture analysis, which means that it basically analyzes whether there are any specific frequency content in the image in specific directions in a localized region around the point or region of analysis. Gabor filters are directly related to Gabor wavelets, since they can be designed for a number of dilations and rotations. General form of Gabor filter is given in (6).

$$g(x,y,\lambda,\theta,\psi,\sigma,\gamma) = \exp\left(-\frac{x'^2+\gamma^2y'^2}{2\sigma^2}\right) + \exp\left(i(2\pi\frac{x'}{\lambda}+\psi)\right)\ , x' = x\,cos\theta + y\,sin\theta, y' = -x\,sin\theta + y\,cos\theta \quad (6)$$

In this equation λ represents the wavelength of the sinusoidal factor, θ represents the orientation of the normal to the parallel stripes of a Gabor function, Ψ is the phase offset, σ is the standard deviation of the Gaussian envelope and γ is the spatial aspect ratio, and specifies the ellipticity of the support of the Gabor function. We obtained two different angles of GPR data and we transformed to single image by superposition with the angles of θ=80º and 100º (SpatialAspectRatio=0.75,SpatialFrequencyBandwidth'=1.5), to compensate varying height affect.

3. EXPERIMENTAL RESULTS

We used a real dataset collected from a soil for 5 types of buried objects. Total data number is 100. List of the buried objects and burial depths are given in Table-4. Antenna height changes 5 cm to 15 cm during data collection in 1 meter cross track. Number of A-scan in each GPR data is approximately M=245. Length of each A-scan is N=256. Detection method parameters are K=7 and P=15. Sample raw GPR B-scan images are given in Figure-6. The results of the methods listed in Table-1 are given from Figure-7 to Figure-19. Receiver Operating Characteristics (ROC) of the methods are also given in Figure-20.

Table-4 List of buried objects used in the tests.

Objects name	Burial depth	Number of data
M14 simulant	9	20
TS50 Simulant	7	20
Metal disk (diameter: 5cm)	10	20
VS50 simulant	10	20
M7A2 simulant	25	20
	TOTAL	100

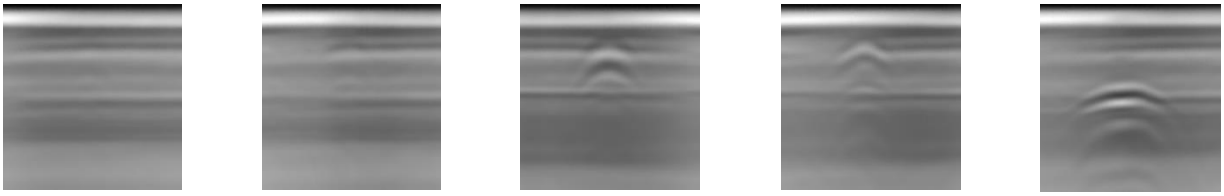

Figure-6 Sample raw GPR data.

4. CONCLUSION

We applied horizontal filtering at each depth line of B-Scan data, to remove varying height effect of antenna. Moreover, we used 1-D Meyer and Haar wavelets to filter out undesired signals from A-scan signals, 2-D Wavelet transform and Gabor filtering to enhance 2-D representation of B-scan data. We obtained different methods (13 methods) by taking a few combinations of main processes.

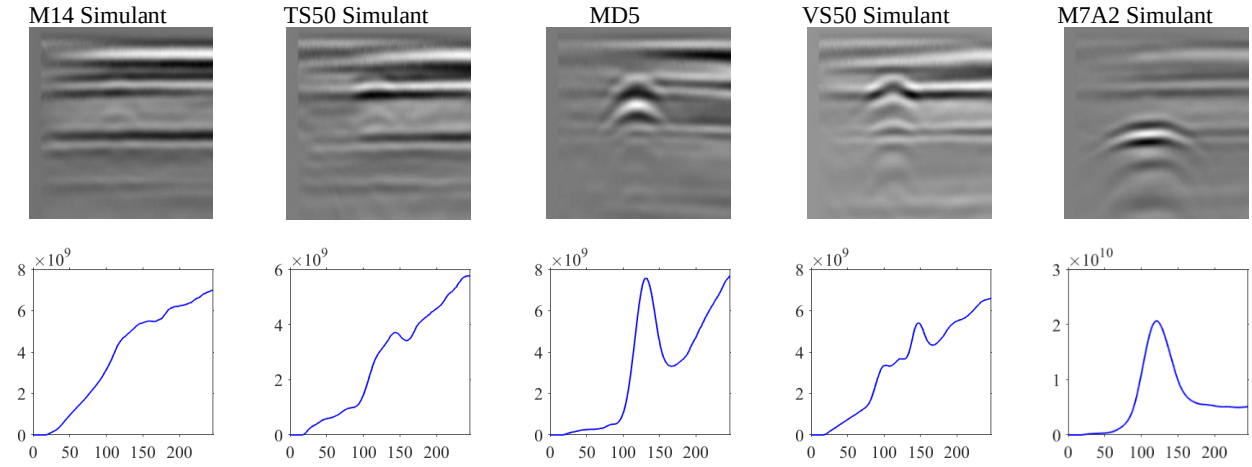

Figure-7 Sample results of Method-1 (constant background removal),
first row: processed GPR data, second row: DTS.

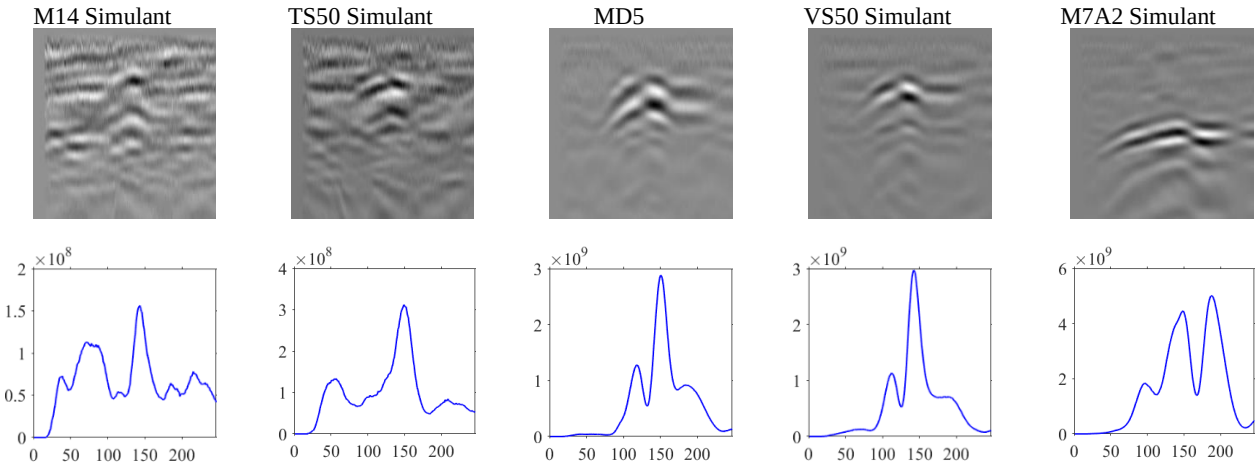

Figure-8 Sample results of Method-2 (constant background removal + horizontal filtering),
first row: processed GPR data, second row: DTS.

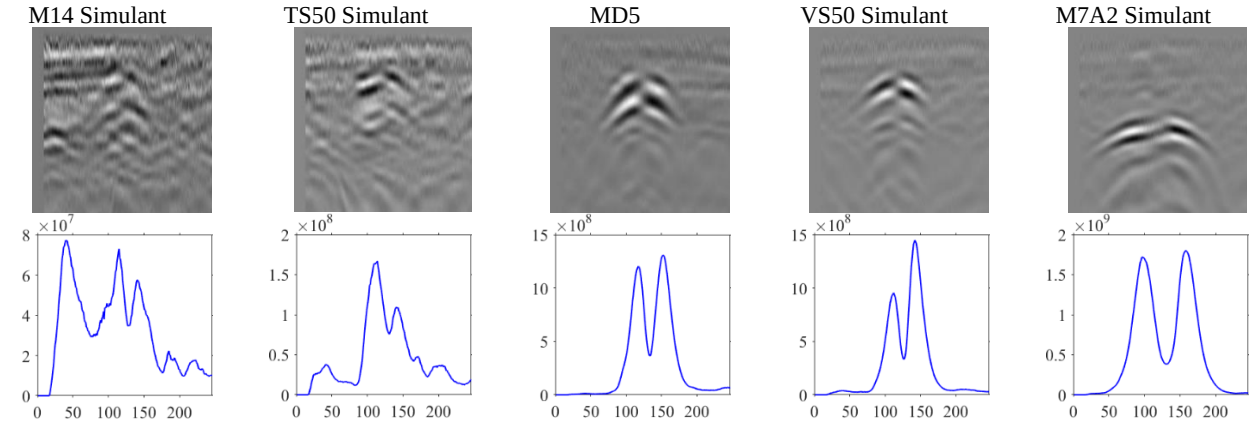

Figure-9 Sample results of Method-3 (moving background removal),
first row: processed GPR data, second row: DTS.

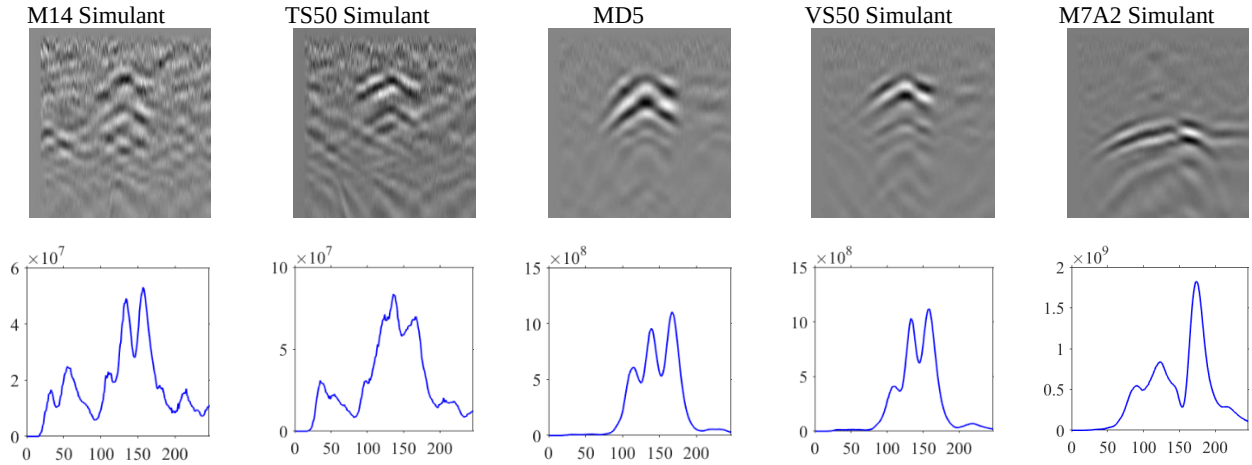

Figure-10 Sample results of Method-4 (moving background removal + horizontal filtering), first row: processed GPR data, second row: DTS.

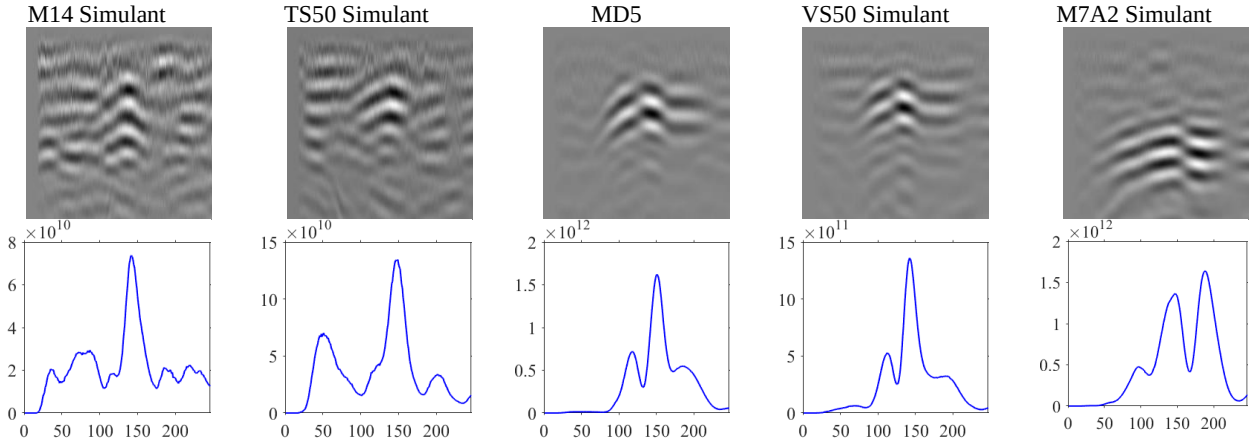

Figure-11 Sample results of Method-5 (constant background removal + horizontal filtering + Meyer wavelet), first row: processed GPR data, second row: DTS.

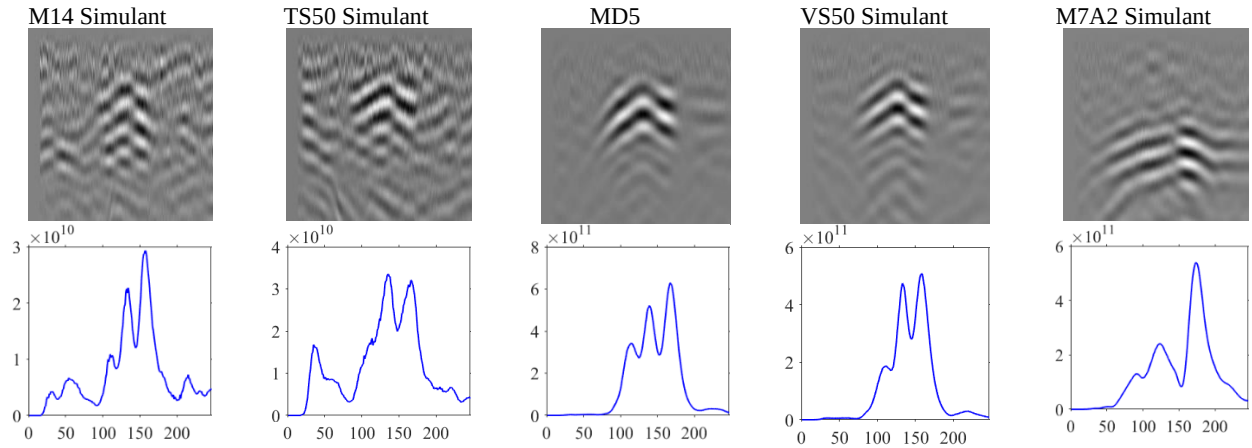

Figure-12 Sample results of Method-6 (moving background removal + horizontal filtering + Meyer wavelet), first row: processed GPR data, second row: DTS.

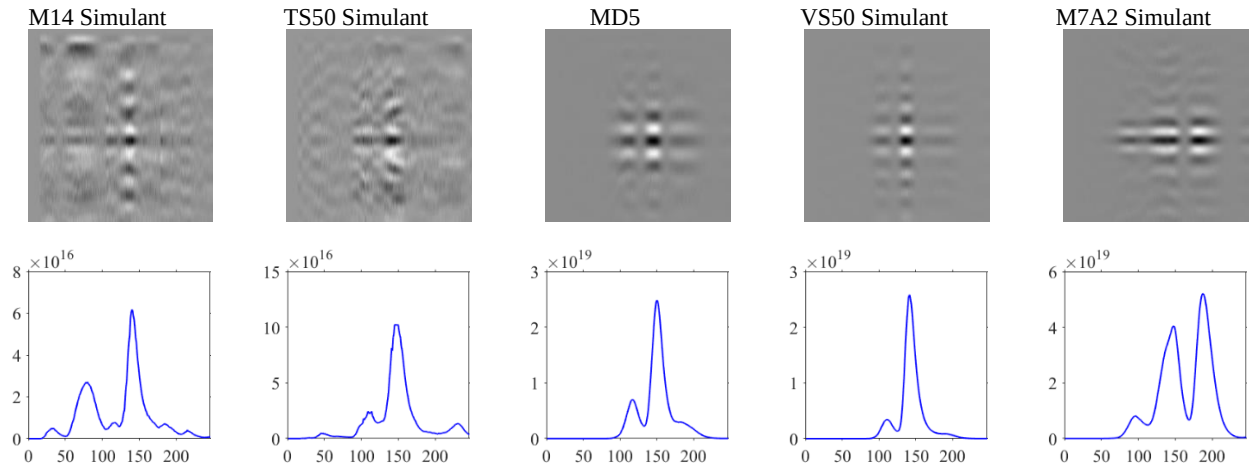

Figure-13 Sample results of Method-7 (constant background removal + horizontal filtering + Haar wavelet), first row: processed GPR data, second row: DTS.

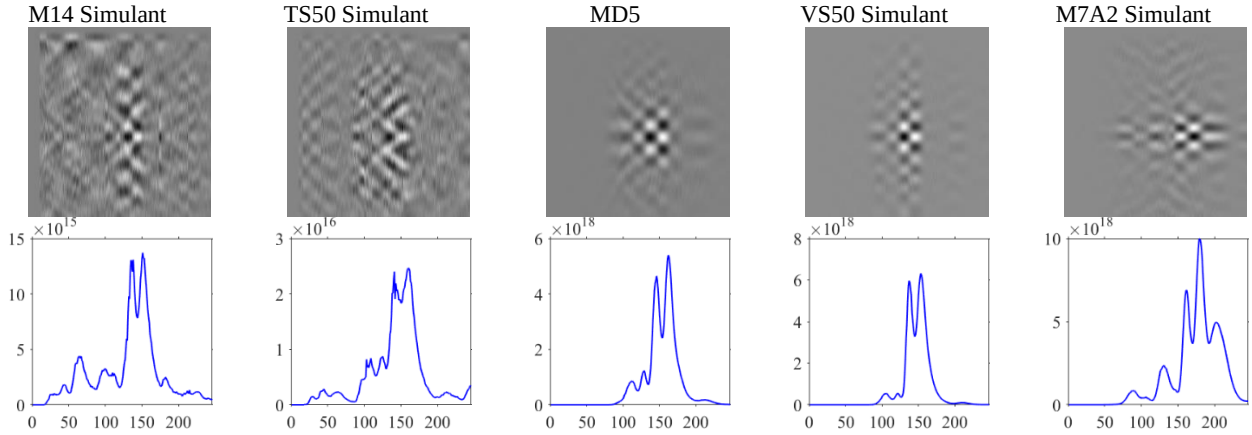

Figure-14 Sample results of Method-8 (moving background removal + horizontal filtering + Haar wavelet), first row: processed GPR data, second row: DTS.

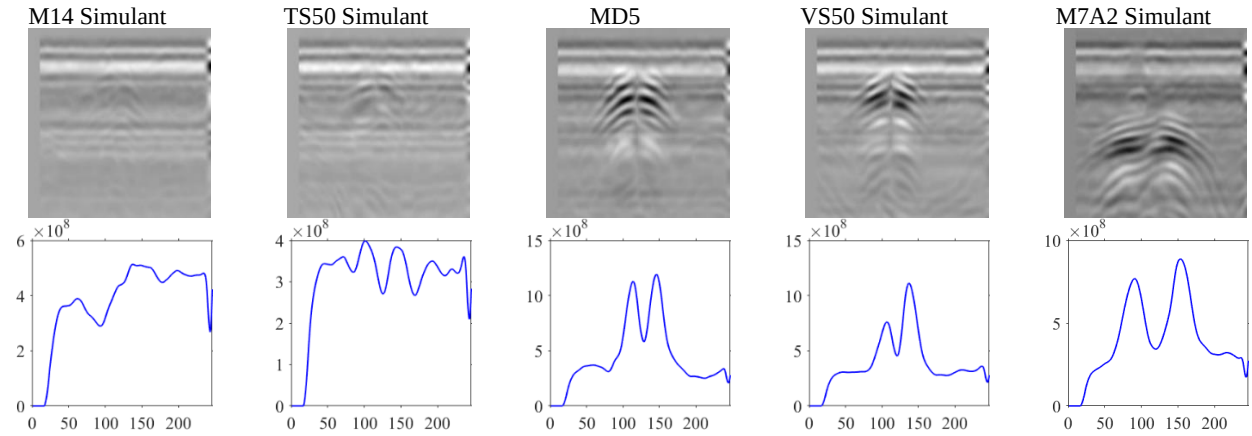

Figure-15 Sample results of Method-9 (constant background removal + 2-D wavelet), first row: processed GPR data, second row: DTS.

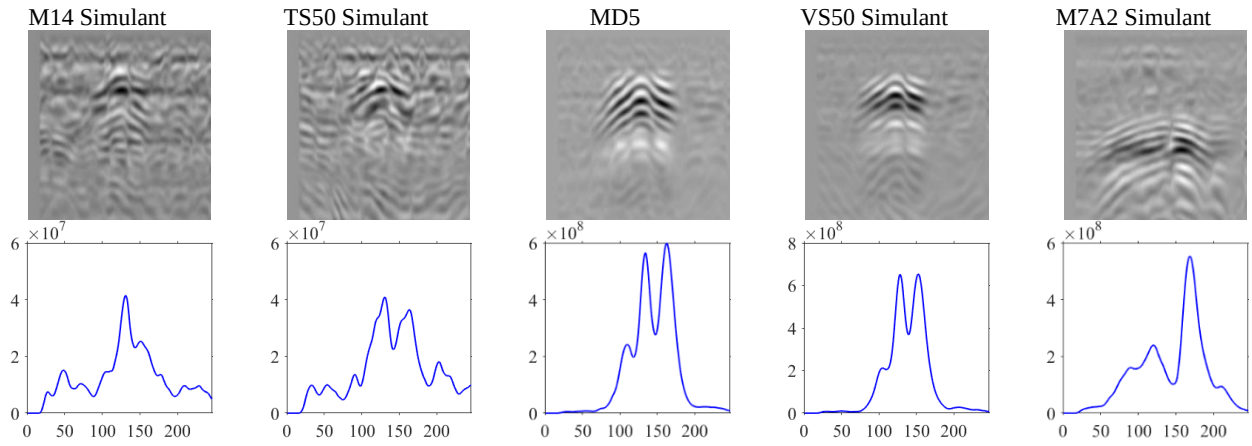

Figure-16 Sample results of Method-10 (constant background removal + horizontal filtering + 2-D wavelet), first row: processed GPR data, second row: DTS.

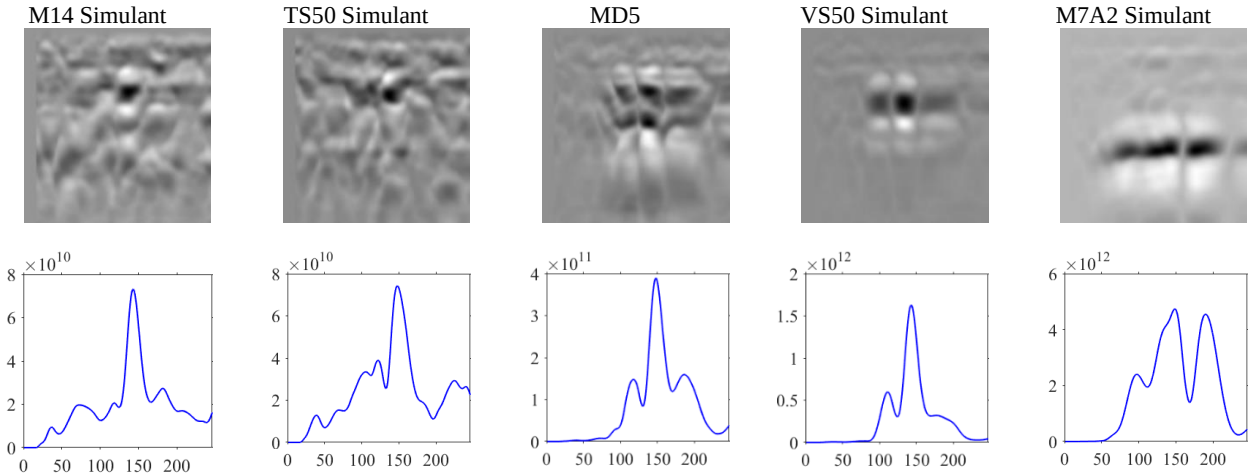

Figure-17 Sample results of Method-11 (constant background removal + horizontal filtering + Gabor filtering), first row: processed GPR data, second row: DTS.

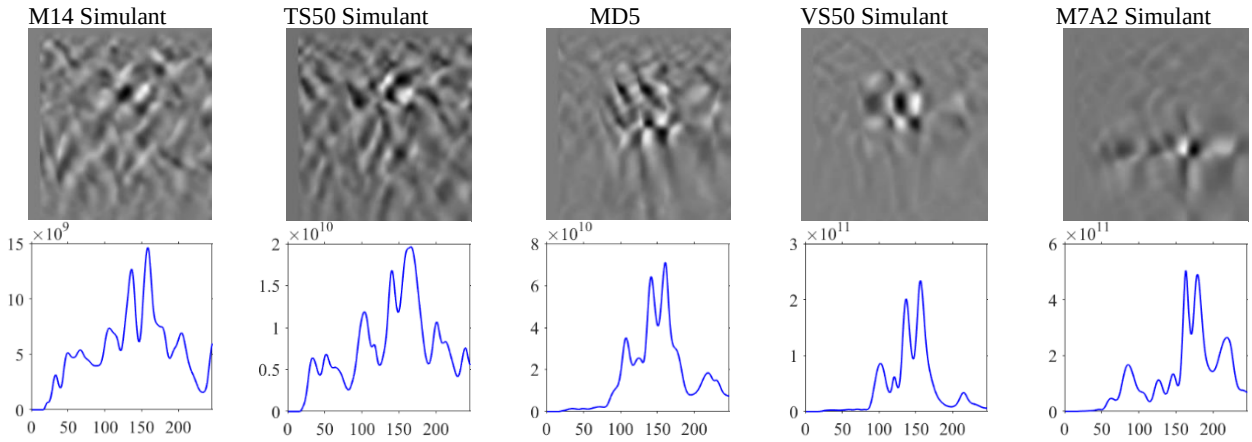

Figure-18 Sample results of Method-12 (moving background removal + horizontal filtering + Gabor filtering), first row: processed GPR data, second row: DTS.

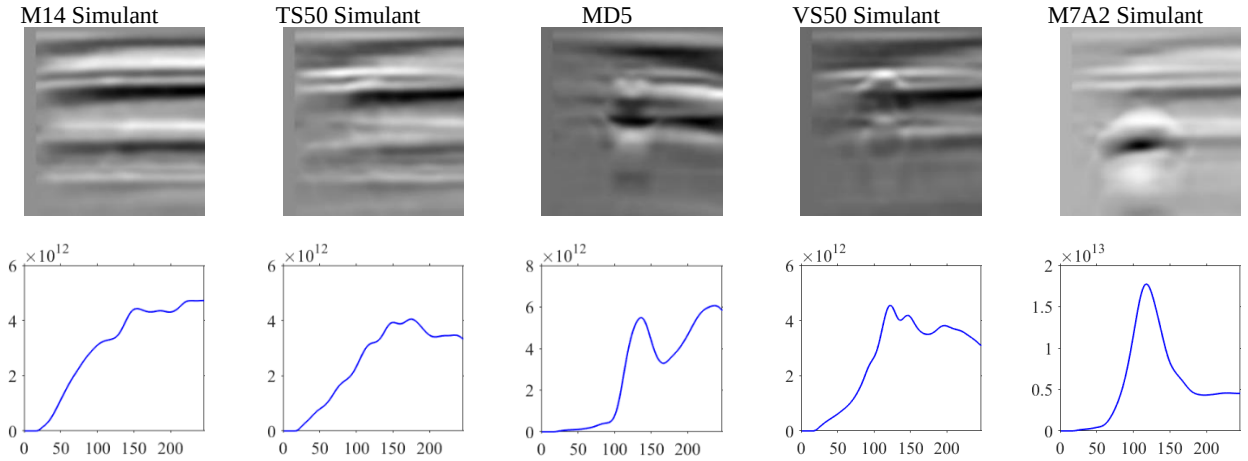

Figure-19 Sample results of Method-13 (constant background removal + Gabor filtering), first row: processed GPR data, second row: DTS.

When we consider **the moving background subtraction-based methods**, we obtain that, Method-3 is the fastest Method to reach 100% detection rate, Method-4 is the second one to reach 100% detection rate (see Figure-20(a)). If we consider **the constant background subtraction-based methods**, we obtain that, Method-7 and Method-11 reach 100% detection rate with approximately the same behavior. However, Method-7 can reach 0% false alarm rate (see Figure-20(d)), while Method-11 cannot reach. Method-10 seems to be a good one in terms of low false alarms with a high detection rate, and this method also produces easily interpretable GPR image (see Figure-16).

When we consider **the category that doesn't use horizontal filtering**, we obtain that, Method-3 is again the fastest Method to reach 100% detection rate, Method-13 is the second one to reach 100% detection rate but degrades spatial information (see Figure-20(c)). If we consider **the category that use horizontal filtering**, we obtain that, Method-7 and Method-11 reach 100% detection rate with approximately the same behavior. However, Method-7 can reach 0% false alarm rate, while Method-11 cannot reach. Method-10 seems to be a good one in terms of low false alarms with a high detection rate (see Figure-20(d)), and this method also produces easily interpretable GPR image (see Figure-16).

When we consider all **13 methods in terms of ROCs given in** Figure-20(d), we obtain that, Method-2, Method-3 and Method-7 reaches 0% false alarm rate with different detection rates but the other methods do not reach. Method-7 and Method-11 has a comparable performance, however, Method-7 can reach 0% false alarm rate with 88% detection rate, while Method-11 cannot reach. When we consider the results of Method-7, we see some degradation in the GPR B-scan images, but we obtain sharper and bigger peaks on detection test statistics function, corresponding to the target location. Although Method-3 is the fastest Method to reach 100% detection rate, may create degradation in GPR images. **Method-10 seems to be a good one in terms of low false alarms with a high detection rate. At the same time, this method produces easily interpretable GPR image of buried object even at the varying antenna height situation**.

A preprocessing method based on horizontal filtering in B-scan data and the use of continuous wavelet transform over A-scan signals is presented, 2-D wavelets and Gabor filter are also applied to GPR data, to solve varying antenna height problem. Comparative results are given over the actual data set obtained from various scenarios. It is observed that the horizontal filtering gives satisfactory results especially in cases where there is variability in antenna height. At the same time 2-D wavelet processing makes easy interpretation of GPR images.

REFERENCES

[1] D.J Daniels, "Ground penetrating radar", IEE Radar Sonar Navigation Avionics Series.15, 254–255, 2004.
[2] Sezgin M., 'Simultaneous buried object detection and imaging utilizing fuzzy weighted background calculation and target energy moments on ground penetrating radar data', EURASIP J. Adv. Signal Process. 2011;2011(1):55.

[3] Daniel Orfeo, Yu Zhang, Dylan Burns, Jonathan Miller, Dryver Huston, Tian Xia, 'Bistatic antenna configurations for air-launched ground penetrating radar', Journal of Applied Remote Sensing Vol. 13, Issue 2, April, 2019.
[4] Monica Di Prinzioa Marco Bittellib Attilio Castellarina Paola Rossi Pisab, 'Application of GPR to the monitoring of river embankments', Journal of Applied Geophysics Volume 71, Issues 2–3, June 2010, Pages 53-61
[5] J. Hugenschmidt, 'Railway track inspection using GPR', Journal of Applied Geophysics V: 43, Issues 2–4, March 2000, P: 147-155
[6] Georgios Kouros et al, '3D Underground Mapping with a Mobile Robot and a GPR Antenna', 2018 IEEE/RSJ International Conference on Intelligent Robots and Systems (IROS).
[7] Motoyuki Sato, 'Dual sensor ALIS evaluation test in Cambodia', Proc. SPIE. 11012, Detection and Sensing of Mines, Explosive Objects, and Obscured Targets XXIV, 2019.
[8] Motoyuki Sato, Kazunori Takahashi Proc, 'Hand-held dual-sensor ALIS and its evaluation tests'. SPIE. 6953, Detection and Sensing of Mines, Explosive Objects, and Obscured Targets XIII, 2008
[9] Sezgin M., 'Development of dual sensor hand-held detector', In: Proceedings of SPIE – detection and sensing of mines, explosive objects, and ob-scured targets XV. Orlando, FL, USA; 2010.
[10] Yoldemir A.B., Sezgin M. 'A least squares approach to buried object detection using ground penetrating radar', IEEE Sensors J. 2011;11(6):1337–1341.
[11] KC Ho, PD Gader, 'A linear prediction land mine detection algorithm for hand held ground penetrating radar', IEEE Trans Geosci. Remote Sens. 40(6), 1374–1384 (2002).
[12] B. Yoldemir, M. Sezgin, 'Peak scatter-based buried object identification using GPR-EMI dual sensor system,' Nondestructive Testing and Evaluation, Taylor and Francis, vol. 34, issue 4, 2019
[13] St´ephane Mallat, 'A Wavelet Tour of Signal Processing', Elsevier,2009
[14] JP Antoine, R Murenzi, 'Two-dimensional directional wavelets and the scale-angle representation' Signal process., 1996, Citeseer
[15] Jean-Pierre Antoine, Romain Murenzi, Pierre Vandergheynst, Syed Twareque Ali, 'Two-Dimensional Wavelets and their Relatives' Cambridge University Press, 2008.
[16] Richard Szeliski, "Computer Vision: Algorithms and Applications" Springer-Verlag London, 2011

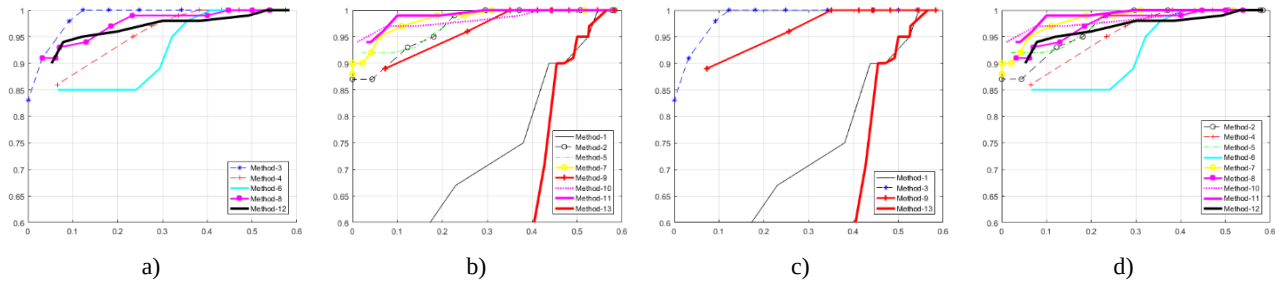

a) b) c) d)

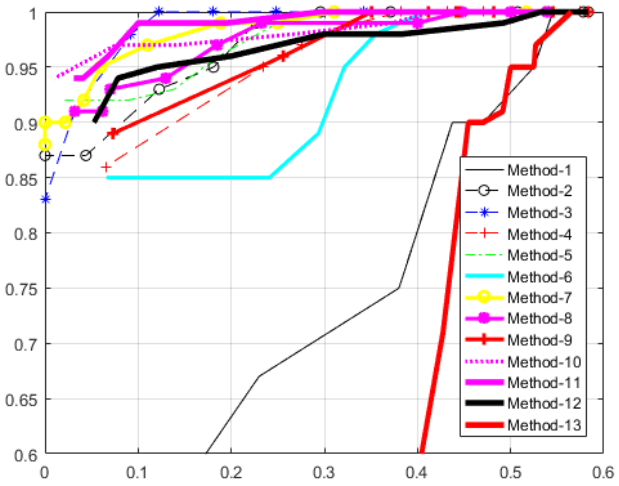

e)

Figure-20. ROC curves of the methods, a) ROCs of the category that use moving background subtraction, b) ROCs of the category that use constant background subtraction, c) ROCs of the category that doesn't use horizontal filtering, d) ROCs of the category that use horizontal filtering, e) ROCs of all 13 methods.